Journal of Nuclear Medicine, published on May 1, 2020 as doi:10.2967/jnumed.119.241364

Molecular imaging of PD-L1 expression and dynamics with the adnectin-based PET tracer ^{18}F-BMS-986192

Thijs S. Stutvoet*[1], Elly L. van der Veen*[1], Arjan Kol[1], Inês F. Antunes[2], Erik F.J. de Vries[2], Geke A.P. Hospers[1], Elisabeth G.E. de Vries[1], Steven de Jong[1], Marjolijn N. Lub-de Hooge[2,3]

[1]Departments of Medical Oncology, [2]Nuclear Medicine and Molecular Imaging, [3]Clinical Pharmacy and Pharmacology, University of Groningen, University Medical Center Groningen, Hanzeplein 1, 9713 GZ Groningen, The Netherlands.

*Both authors contributed equally

Address of correspondence:

Marjolijn Lub-de Hooge, PharmD, PhD,

Department of Clinical Pharmacy and Pharmacology,

University Medical Center Groningen, P.O. Box 30.001,

9700 RB Groningen,

the Netherlands.

Tel. +31503614071, Fax. +31503614087

E-mail: m.n.de.hooge@umcg.nl

First authors:

Thijs S. Stutvoet, MD, PhD student,

Department of Medical Oncology

University Medical Center Groningen, P.O. Box 30.001,

9700 RB Groningen, the Netherlands.

Tel. +31-6-51453833; Fax. +31-50-3611687

E-mail: t.s.stutvoet@umcg.nl

Elly L. van der Veen, PharmD, PhD student,

Department of Medical Oncology

University Medical Center Groningen, P.O. Box 30.001,

9700 RB Groningen, the Netherlands.

Tel. +31-50-3610871; Fax. +31-50-3611687

E-mail: e.l.van.der.veen@umcg.nl

Short running title: PD-L1 PET imaging with ^{18}F-BMS-986192

Funding

Thijs S. Stutvoet is supported by a fellowship of the Junior Scientific Master Class of the University of Groningen.

Word count: 4986

ABSTRACT

^{18}F-BMS-986192, an adnectin-based human programmed cell death ligand 1 (PD-L1) tracer, was developed to non-invasively determine whole-body PD-L1 expression by positron emission tomography (PET). We evaluated usability of ^{18}F-BMS-986192 PET to detect different PD-L1 expression levels and therapy-induced changes of PD-L1 expression in tumors. **Methods:** *In vitro* binding assays with ^{18}F-BMS-986192 were performed in human tumor cell lines with different total cellular and membrane PD-L1 protein expression levels. Subsequently, PET imaging was executed in immunodeficient mice xenografted with these cell lines. Mice were treated with interferon gamma (IFNγ) intraperitoneally for 3 days or with the mitogen-activated protein kinase kinase (MEK1/2) inhibitor selumetinib by oral gavage for 24 hours. Thereafter ^{18}F-BMS-986192 was administered intravenously, followed by a 60-minute dynamic PET scan. Tracer uptake was expressed as percentage injected dose per gram tissue (%ID/g). Tissues were collected to evaluate *ex vivo* tracer biodistribution and to perform flow cytometric, Western blot, and immunohistochemical tumor analyses. **Results:** ^{18}F-BMS-986192 uptake reflected PD-L1 membrane levels in tumor cell lines, and tumor tracer uptake in mice was associated with PD-L1 expression measured immunohistochemically. *In vitro* IFNγ treatment increased PD-L1 expression in the tumor cell lines and caused up to 12-fold increase in tracer binding. *In vivo,* IFNγ did neither affect PD-L1 tumor expression measured immunohistochemically nor ^{18}F-BMS-986192 tumor uptake. *In vitro,* selumetinib downregulated cellular and membrane levels of PD-L1 of tumor cells by 50% as measured by Western blotting and flow cytometry. In mice, selumetinib lowered cellular, but not membrane PD-L1 levels of tumors and consequently no treatment-induced change in ^{18}F-BMS-986192 tumor uptake was observed. **Conclusion:** ^{18}F-

BMS-986192 PET imaging allows detection of membrane-expressed PD-L1, as soon as 60 minutes after tracer injection. The tracer can discriminate a range of tumor cell PD-L1 membrane expression levels.

Keywords: molecular imaging, positron emission tomography, programmed death ligand-1, ^{18}F-labeled adnectin, ^{18}F-BMS-986192

INTRODUCTION

Programmed cell death protein 1 (PD-1) / programmed death ligand 1 (PD-L1) inhibitors have radically improved treatment of patients with cancer. These drugs have been approved for treatment of many tumor types and for unresectable and metastatic microsatellite instability–high or metastatic mismatch repair deficient solid tumors (*1*). Combining a PD-1 antibody with the cytotoxic T-lymphocyte-associated protein 4 antibody ipilimumab increases efficacy in melanoma (*2*). In addition, numerous studies aim to improve efficacy by combining PD-1/PD-L1 antibodies with novel immune checkpoint inhibitors, targeted agents, chemotherapies and radiotherapy (*3*).

Despite impressive antitumor effects, many patients do not respond to PD-1/PD-L1 targeted treatment. Still, these patients are at risk for side effects (*4*,*5*). To select patients that are most likely to respond to immune checkpoint inhibitors, immunohistochemical quantification of tumor cell PD-L1 expression can be performed (*6*). However, discrepancy between PD-L1 status and tumor response occurs (*7*,*8*). Immunohistochemistry of a single tumor biopsy may fail to capture the heterogeneity of PD-L1 expression within and between lesions and changing expression over time (*9*–*12*).

Positron emission tomography (PET) is a potential method to non-invasively evaluate whole-body PD-L1 expression levels. Radiolabeled antibodies targeting PD-1 or PD-L1 have been used in this context (*7*,*13*,*14*). Imaging with radiolabeled antibodies requires several days of tracer clearance from circulation to obtain PET images with adequate contrast (*13*). Given their fast tumor penetration and short serum half-lives, radiolabeled small molecules targeting PD-L1 could yield adequate contrast for imaging within one hour, allowing imaging on the day of

tracer injection (*7*). The ~12 kDa adnectin-based human PD-L1 targeting PET tracer ^{18}F-BMS-986192 has been developed for this purpose (*15*). In preclinical studies ^{18}F-BMS-986192 imaging allowed distinction of a PD-L1 positive from a negative tumor within 2 hours after tracer injection (*16*).

Here, we aimed to evaluate whether ^{18}F-BMS-986192 PET can be used to distinguish different intrinsic PD-L1 expression levels in tumor cell lines and tumor xenografts in mice. Moreover, we investigated whether ^{18}F-BMS-986192 PET can be used to detect therapy-induced modulation of PD-L1 expression levels. *Ex vivo* analysis of tumor tissue using flow cytometry, Western blot, and immunohistochemistry was performed to evaluate PD-L1 expression levels.

MATERIALS AND METHODS

Cell Lines And Reagents

The human tumor cell lines H292 (lung mucoepidermoid carcinoma) and H358 (lung adenocarcinoma) were obtained from the American Type Culture Collection, H322 (human lung adenocarcinoma) was obtained from Sigma-Aldrich and ES2 (human ovarian clear cell carcinoma) was a kind gift from Dr. Els Berns (Erasmus MC, The Netherlands). All cells were cultured in RPMI 1640 (Invitrogen) medium with 10% fetal calf serum (Bodinco BV) (supplemented with 2 mM L-glutamine for H322 cells) and maintained in a humidified atmosphere with 5% CO_2 at 37°C. Cells were regularly tested for mycoplasma contamination and were proven to be mycoplasma negative. Cell line authentication was regularly performed using short tandem repeat profiling.

Tracer Production

The human PD-L1 specific PET tracer ^{18}F-BMS-986192 was produced with a radiochemical purity >90% and molar activity of >6100 GBq/mmol according to a slightly modified version of a previously published protocol (supplementary methods, (*16*)). In short, ^{18}F-BMT-187144 is formed by fluorination of the precursor BMT-180478-01 (Bristol-Myers Squibb) with ^{18}F-fluoride. Next, ^{18}F-BMS-986192 is generated by a [2,3]-cycloaddition reaction of the cyclooctyne moiety in the anti-PD-L1 adnectin precursor BMT-192920 (Bristol-Myers Squibb) with the azide group in ^{18}F-BMT-187144. Ultra-high performance liquid chromatography was used to determine (radio)chemical purity, radiochemical identity and molar activity (supplementary methods). *In vitro* and *in vivo* tracer stability were demonstrated previously (*16*).

Tracer Binding Studies

For binding assays, 0.1 x 10^6 cells were grown for 24 hours in RPMI medium with 10% fetal calf serum in 24-well plates and treated with the inducer of PD-L1, interferon-γ (IFNγ, R&D systems) with a final concentration up to 6 *10^5 IU/mL (30 ng/mL, diluted in sterile water) (*17*). Tracer (1 MBq, 50 µL, 3330 ng/mL, 167 ng) was added to each well and cells were incubated for 60 minutes at 37˚C. Competition assays were performed by adding 50 µL of a mixture of 1400 ng/mL tracer solution with increasing amounts of non-radioactive ^{19}F-BMS-986192 (from 5 ng/mL to 4*10^5 ng/mL) to each well. After incubation, cells were washed twice with 1 mL ice-cold phosphate buffered saline (PBS: 9.7 mM Na_2HPO_4, 1.6 mM KH_2PO4, 150 mM NaCl, pH = 7.2) containing 1% human serum albumin. Cells were trypsinized and medium was added. Cell suspensions were transferred to plastic tubes. Radioactivity in the cell fraction was measured in

a gamma counter (Wizard^2 2480-0019, SW 2.1, PerkinElmer). To correct for IFNγ-induced cytotoxicity, radioactivity was corrected for the number of viable cells, counted using trypan blue and expressed as counts/minute per 100,000 cells. Binding assays were performed in triplicate as a single assay. For modulation experiments tumor cell lines were treated with 10 µM of the mitogen-activated protein kinase kinase (MEK) 1/2 inhibitor selumetinib (AZD6244, Axon Medchem) for 24 hours before analysis. Modulation experiments were performed in three independent biological replicates.

Animal Studies

Animal studies were performed according to Dutch Regulations for Animal Welfare. The protocol was approved by the animal ethical committee of the University of Groningen. To assess tracer binding *in vivo*, 5 to 8 weeks old immune deficient BALB/c nude mice (BALB/cOlaHsd-Foxn1nu, Envigo) were subcutaneously inoculated with tumor cells in a mixture of Matrigel (high protein concentration, Corning) and PBS (H292: $5x10^6$ in 300 µL Matrigel/PBS (1:1); H358 $2x10^6$ in 300 µL Matrigel/PBS (1:1); $5x10^6$ ES2 cells in 300 µL PBS). Tumor size and animal weight were measured two times per week. When tumors were 100-200 mm^3 treatment and PET imaging studies were performed.

Treatment Studies

Mice xenografted with H292 cells were randomized between vehicle (diluent only) and IFNγ treatment. Recombinant human IFNγ was administered at different daily doses ($1x10^3$, $1x10^4$ and $1x10^5$ IU, corresponding to 0.05, 0.5 and 5 µg, 5-6 mice per group) by intraperitoneal injection once daily for 3 days. On day 3 PET imaging studies were performed.

Mice xenografted with ES2 cells were randomized between vehicle treatment (diluent only) and selumetinib treatment groups (4-5 mice per group). Selumetinib was diluted in 0.2% Tween-80 and 0.5% hydroxyl-propyl methylcellulose (Sigma-Aldrich) and administered at 10 mg/kg twice daily by oral gavage, starting 24 hours before PET scanning. This was based on earlier research indicating minimal effects on tumor growth at this concentration (*18*).

PET Studies

For PET imaging ^{18}F-BMS-986192 (8.20 MBq ± 4.74 MBq; average 3 MBq/µg) was injected intravenously via the penile vein. Immediately after tracer injection a 60-minute dynamic PET scan was performed. Mice were placed in a Focus 220 rodent scanner (CTI Siemens) and kept warm on heating mats. After the emission scan, a transmission scan of 515 seconds was performed using a ^{57}Co point source to correct for scatter, random coincidences and tissue attenuation. After the scan, mice were sacrificed for *ex vivo* biodistribution. Organs were dissected, weighed and their radioactivity was measured in a gamma-counter. Uptake in the organs was calculated as percentage of the injected dose per gram of tissue (%ID/g).

PET Reconstruction

PET data was reconstructed into 10-minute frames and *in vivo* quantification was performed using PMOD software (version 4.0, PMOD Technologies LCC, Switzerland). Three-dimensional regions of interest (ROI) were drawn around the tumor, based on *ex vivo* measured tumor volume, and a threshold equal to 40% of the maximum intensity was used to determine uptake. Necrotic parts of the tumor were excluded. For other organs a fixed-size sphere was drawn in representative parts of the organs. Tracer uptake was calculated as the average uptake

in the last frame (50-60 minutes after injection) and presented as %ID/g, based on previous results (*16*).

Ex Vivo And In Vitro Tumor Cell Analyses

For PD-L1 measurements with flow cytometry, xenograft tumors were incubated overnight in RPMI 1640, with 10% fetal calf serum, 16.7 µg/mL DNAse (Roche Diagnostics Nederland B.V.), and 1 mg/mL collagenase IV (Thermo Fischer Scientific) at room temperature. Single cell suspensions were created using 70 µm cell strainers. For *in vitro* PD-L1 measurements, cells growing in monolayer were harvested using trypsin. For both *ex vivo* and *in vitro* cells, 100,000 cells were stained with anti-PD-L1 (clone 29E.2A3, BioLegend) and secondary antibodies against mouse IgG (polyclonal goat anti-mouse PE, SouthernBiotec), or directly stained with pycoerythrin (PE)-labeled anti-PD-L1 (MIH-I, Invitrogen). At least 10,000 events were measured on the Accuri C6 (BD Biosciences) or FACSverse (BD Biosciences) apparatus. Data was analyzed based on mean fluorescence intensity. For Western blotting analysis, xenograft tumors were homogenized using the Bel-Art Micro-Tube Homogenizer (Thermo Fisher Scientific). Lysates from homogenized xenograft tumors and cell lines growing in monolayer were made using mammalian protein extraction reagent with phosphatase and protease inhibitors diluted 1:100 (Thermo Fisher Scientific). Proteins were separated using sodium dodecyl sulfate polyacrylamide gel electrophoresis. Membrane staining was performed with 1:1000 rabbit anti-PD-L1 (E1L3N, Cell Signaling Technology), GAPDH (EPR6256, Abcam), and secondary HRP-anti-mouse or HRP-anti-rabbit antibodies at 1:1500 (Dako). Detection was performed using Lumi-Light Western blotting substrate (Roche Diagnostics Nederland B.V.) and a digital imaging system (Bio-Rad). Quantification of Western blot signals was performed by

measuring relative optical density of the target protein, compared to relative GAPDH optical density using imageJ after subtraction of the background signal.

For immunohistochemistry, formalin fixed paraffin embedded xenograft tumors were cut into 4 µm slices and placed on glass slides. Antigen retrieval was performed using universal heat-induced epitope retrieval reagent (Abcam), followed by endogenous peroxidase block (S2003, Dako), endogenous IgG block (X0909, Dako) and incubation with anti-PD-L1 antibody (clone 28-8, Abcam) for 60 minutes. Next, sections were incubated with anti-rabbit Dako envision+ polymer for 30 minutes (K4010, Dako). The staining was visualized using 3,3'-diaminobenzidine+ substrate (K3468, Dako) and counterstained using hematoxylin.

Statistical Analysis

Data is presented as mean ± standard deviation (SD). A t-test, Kruskal-Wallis test with Dunn's multiple comparisons test, or ANOVA with Bonferroni's multiple comparisons test was performed to compare groups (GraphPad, Prism 7). P values ≤ 0.05 were considered statistically significant.

RESULTS

^{18}F-BMS-986192 Binding Increases With Higher PD-L1 Expression

To study the ability of ^{18}F-BMS-986192 to detect a range of PD-L1 levels, we selected 4 tumor cell lines with different basal PD-L1 membrane expression levels *in vitro* as measured by flow cytometry (Fig. 1A). Binding assays confirmed 2-fold increased binding of ^{18}F-BMS-986192 to H358 cells, compared to H292 cells, corresponding to the difference in basal PD-L1 expression (Supplemental Fig. 1A). Tracer binding could be blocked by adding non-radioactive ^{19}F-BMS-

986192, indicating specific binding (Supplemental Fig. 1B). *In vivo* PET experiments were performed with xenograft models of H292, H358 and ES2. ^{18}F-BMS-986192 uptake in the different xenograft models when measured with PET imaging (%ID/g ± SD H292: 1.33 ± 0.37, H358: 1.62 ± 0.86, ES2: 2.36 ± 1.07) and *ex vivo* biodistribution (%ID/g ± SD H292: 1.64 ± 0.60, H358: 2.81 ± 1.84, ES2: 4.25 ± 2.3) was associated with PD-L1 expression (Figs. 1B and 1C). Western blot and immunohistochemical analysis confirmed the differential PD-L1 expression levels *in vivo*, with ES2 showing the highest PD-L1 levels (Figs. 1D and 1E). Tracer levels in other organs were low, except at the site of renal excretion (Supplemental Figs. 1C and 1D).

^{18}F-BMS-986192 Tumor Uptake Reflects Failure Of IFNγ To Induce PD-L1 Expression *In Vivo*

We have previously demonstrated that the pro-inflammatory cytokine IFNγ activates the IFNγ signaling pathway and increases both total protein and membrane levels of PD-L1 in H292 and H358 cells *in vitro* (*19*). In the present study, these cell lines showed increased tracer binding after 24 hour treatment with IFNγ *in vitro* (Supplemental Fig. 2A). Both *in vivo* PET results and *ex vivo* analyses showed a minor trend towards higher ^{18}F-BMS-986192 uptake in H292 tumors after treatment of the mice with up to 10^5 IU IFNγ daily for 3 days (Fig. 2A). Treatment did not influence tumor volume (data not shown). In other organs no difference in tracer distribution was observed (Supplemental Figs. 2B and 2C). Western blot and immunohistochemistry confirmed that IFNγ treatment failed to increase PD-L1 expression in tumors, with only a non-significant increase of IFNγ-signaling protein pSTAT1, a known activator of PD-L1 transcription (Figs. 2B and 2C).

^{18}F-BMS-986192 Tumor Uptake Reflects Failure Of Selumetinib To Reduce Tumor Cell PD-L1 Membrane Expression Levels *In Vivo*

Next, we investigated whether ^{18}F-BMS-986192 could detect treatment-induced downregulation of PD-L1. *In vitro* treatment of the strongly PD-L1 positive ES2 cells with selumetinib for 24 hours resulted in a complete blockade of MEK1/2 signaling and ~50% downregulation of PD-L1 membrane expression levels and total PD-L1 protein expression (Fig. 3A). *In vivo* and *ex vivo* analyses showed that 1 day treatment with 10 mg/kg selumetinib by oral gavage did not affect ^{18}F-BMS-986192 tumor uptake or biodistribution compared to vehicle-treated mice (Figs. 3B; Supplemental Figs. 3A and 3B). Moreover, flow cytometric analysis confirmed that selumetinib treatment did not lead to a reduction of tumor cell PD-L1 membane expression levels (Fig. 3C). E*x vivo* analysis, however, showed that the treatment effectively inhibited MEK1/2 signaling and cellular PD-L1 expression (Figs. 3D and 3E). Treatment did not influence tumor volume (data not shown). These results indicate that ^{18}F-BMS-986192 specifically detects PD-L1 membrane levels and that tracer uptake is not influenced by cellular PD-L1 levels.

DISCUSSION

In this study, we assessed the utility of ^{18}F-BMS-986192 PET to non-invasively measure PD-L1 expression levels. ^{18}F-BMS-986192 tumor uptake was related to basal PD-L1 expression in cell lines and in xenograft models, enabling non-invasive detection of differential PD-L1 membrane levels. Selumetinib treatment reduced cellular PD-L1 expression. However, PD-L1 membrane levels were not altered by treatment with IFNγ or selumetinib. Tracer uptake was not affected by treatment, suggesting that ^{18}F-BMS-986192 PET reflects membrane levels, rather than cellular expression, of PD-L1.

This is the first study demonstrating that same-day PET imaging with an adnectin-based tracer discriminates low from moderate and high tumor cell PD-L1 expression using preclinical *in vivo* models. ^{18}F-BMS-986192 can detect 2-fold differences in PD-L1 membrane levels. Tumor uptake of ^{18}F-BMS-986192, expressed as %ID/g, is lower than uptake with monoclonal antibody based tracers, however similar to results in other preclinical studies evaluating same-day imaging of PD-L1 (*20–24*). ^{18}F-BMS-986192 is specific for human PD-L1, with picomolar dissocation constants (K_D<35 pM). This prevents influence of mouse tissues on tracer uptake (*16*). However, in humanized immune competent models, with human PD-L1 expressing immune cells, tracer distribution might be different. Moreover, in these models and in patients, tracer uptake in the tumor might differ because of increased tumor cell PD-L1 expression and PD-L1 positive tumor immune cell infiltration (*25*).

To study imaging of treatment-induced changes in PD-L1 expression, we aimed to modulate PD-L1 expression levels in tumor xenografts. IFNγ, a well-known inducer of tumor cell PD-L1 expression *in vitro* (*26*), failed to increase tumor cell PD-L1 expression *in vivo*. Although intravenous administration of IFNγ increases mouse lung PD-L1 expression and intraperitoneal administration of IFNγ sensitizes xenograft models for pemetrexed, direct evidence of tumor cell PD-L1 upregulation by IFNγ *in vivo* is sparse (*4*,*27*,*28*). PD-L1 expression is regulated on many levels, so it may be that factors critical for PD-L1 upregulation are missing in the tumor microenvironment of H292 xenografts (*4*). Additionally, we aimed to reduce PD-L1 expression of tumors by treatment with selumetinib. Despite reduced total PD-L1 protein levels, PD-L1 membrane levels and tumor ^{18}F-BMS-986192 uptake were not affected after treatment *in vivo*. Multiple post-translational mechanisms, including altered recycling of PD-L1 to the cell

membrane, may give rise to the lack of correlation between total PD-L1 protein levels and PD-L1 membrane levels (*29–32*). In our model the reduction of total protein levels *in vivo* may be followed by a delayed reduction in PD-L1 membrane levels, after the 24 hour time point. In addition, tracer uptake corresponded better with PD-L1 membrane expression than with total protein levels of PD-L1 (Supplemental Figure 4). These modulation experiments show the challenges of studying immune checkpoint biology in preclinical models. The complex interaction between cell types in the tumor microenvironment is suboptimally reflected in mouse models, urging critical evaluation of clinical validity of preclinical findings. However, we were still able to detect different tumor cell PD-L1 levels, indicating that serial imaging with this tracer in patients may provide insight into treatment effects on PD-L1 membrane levels. Interestingly, the majority of approved PD-L1 immunohistochemical assays measure the membrane-bound fraction of PD-L1, because this is hypothesized to be immunologically most active (*33*).

Clinically, PD-L1 imaging has the potential to predict response to immunotherapy better than PD-L1 immunohistochemistry, as shown in the first-in-human clinical study with the anti-PD-L1 monoclonal antibody ^{89}Zr-atezolizumab (*34*). Comparing ^{89}Zr-atezolizumab imaging with a clinical study using ^{18}F-BMS-986192, results suggest that this PD-L1 antibody-based PET tracer reaches higher target uptake levels than ^{18}F-BMS-986192 (*34*,*35*). However, the short serum half-life and rapid diffusion of ^{18}F-BMS-986192 enable same-day imaging with high contrast images, and reduce radiation burden (*35*,*36*). This might allow rapid follow-up of treatment-induced changes of PD-L1 expression with PET imaging. Also, it enables combined PET imaging of multiple targets on subsequent days, providing more information. Feasibility of imaging

multiple immunotherapy-related targets in a single patient was shown in a small study using ^{18}F-BMS-986192 in combination with PD-1 targeting ^{89}Zr-nivolumab in 13 patients (*35*). Currently, ^{18}F-BMS-986192 is further being investigated in metastatic melanoma, NSCLC and oral cancer patients. ^{18}F-BMS-986192 PET imaging is performed at baseline and during nivolumab treatment (ClinicalTrials.gov identifiers NCT03520634 and NCT03843515). In both studies PET uptake will be correlated with PD-L1 expression in biopsy samples measured by immunohistochemistry. Future larger studies will have to define the precise role of PET imaging in predicting tumor response to immune checkpoint inhibitors or to study treatment effects on PD-L1 expression by performing serial imaging.

CONCLUSION

^{18}F-BMS-986192 PET imaging can be used to non-invasively quantify PD-L1 membrane levels. This makes it a potential tool to study PD-L1 expression dynamics and predict responses to immunotherapy. Further clinical evaluation will be necessary to validate these findings in humans.

DISCLOSURE

Competing Interests

E.F.J.d.V. reports grants from ZonMW (no. 95104008, 95105010), and from Dutch Cancer Foundation (no. RUG2015-7235) during the conduct of the study; contract research studies with Rodin Therapeutics, Lysosomal Therapeutics Inc., Hoffmann-La Roche Ltd and Ionis Pharmaceuticals, with funds made available to the institution outside the submitted work; G.A.P.H reports consulting and advisory role for Amgen, Roche, MSD, BMS, Pfizer, Novartis;

grants from BMS, Seerave; made available to the institution outside the submitted work; E.G.E.d.V reports grants from IMI TRISTAN (GA no.116106), during the conduct of the study; consulting and advisory role for NSABP, Daiichi Sankyo, Pfizer, Sanofi, Merck, Synthon Biopharmaceuticals; grants from Amgen, Genentech, Roche, Chugai Pharma, CytomX Therapeutics, Nordic Nanovector, G1 Therapeutics, AstraZeneca, Radius Health, Bayer, all made available to the institution, outside the submitted work. Cooperators at Bristol Meyers Squibb approved the preclinical design and the final version of the manuscript. All remaining authors have declared no conflicts of interest.

Funding

T.S.S. is supported by a fellowship of the Junior Scientific Master Class of the University of Groningen.

ACKNOWLEDGMENTS

The authors would like to thank Ralph Adam Smith, Wendy Hayes, David Leung, David J. Donnelly, Samuel J. Bonacorsi and Paul Morin for their efforts in support of the work generated in this manuscript.

KEY POINTS

Question

Can ^{18}F-BMS-986192 PET be used to detect different PD-L1 expression levels and therapy-induced changes of tumor cell PD-L1 expression?

Pertinent Findings

^{18}F-BMS-986192 PET imaging in immune-competent tumor-bearing mice allows detection of PD-L1 membrane levels, as soon as 60 minutes after tracer injection. The tracer can discriminate a range of tumor cell PD-L1 membrane levels.

Implications For Patient Care

^{18}F-BMS-986192 PET imaging might be a potential tool to study PD-L1 expression dynamics and predict responses to immunotherapy in humans.

REFERENCES

1. Ribas A, Wolchok JD. Cancer immunotherapy using checkpoint blockade. *Science*. 2018;359:1350-1355.
2. Hodi FS, Chiarion-Sileni V, Gonzalez R, et al. Nivolumab plus ipilimumab or nivolumab alone versus ipilimumab alone in advanced melanoma (CheckMate 067): 4-year outcomes of a multicentre, randomised, phase 3 trial. *Lancet Oncol*. 2018;19:1480-1492.
3. Tang J, Shalabi A, Hubbard-Lucey VM. Comprehensive analysis of the clinical immuno-oncology landscape. *Ann Oncol*. 2018;29:84-91.
4. Sun C, Mezzadra R, Schumacher TN. Regulation and function of the PD-L1 checkpoint. *Immunity*. 2018;48:434-452.
5. Nishijima TF, Shachar SS, Nyrop KA, Muss HB. Safety and tolerability of PD-1/PD-L1 inhibitors compared with chemotherapy in patients with advanced cancer: a meta-analysis. *Oncologist*. 2017;22:470-479.
6. Gong J, Chehrazi-Raffle A, Reddi S, Salgia R. Development of PD-1 and PD-L1 inhibitors as a form of cancer immunotherapy: A comprehensive review of registration trials and future considerations. *J Immunother Cancer*. 2018;6:1-18.
7. Broos K, Lecocq Q, Raes G, Devoogdt N, Keyaerts M, Breckpot K. Noninvasive imaging of the PD-1: PD-L1 immune checkpoint: Embracing nuclear medicine for the benefit of personalized immunotherapy. *Theranostics*. 2018;8:3559-3570.
8. Carbognin L, Pilotto S, Milella M, et al. Differential activity of nivolumab, pembrolizumab and MPDL3280A according to the tumor expression of programmed death-ligand-1 (PD-L1): sensitivity analysis of trials in melanoma, lung and genitourinary cancers. Santini D,

ed. *PLoS One*. 2015;10:e0130142.

9. Madore J, Vilain RE, Menzies AM, et al. PD-L1 expression in melanoma shows marked heterogeneity within and between patients: Implications for anti-PD-1/PD-L1 clinical trials. *Pigment Cell Melanoma Res*. 2015;28:245-253.

10. Uruga H, Bozkurtlar E, Huynh TG, et al. Programmed cell death ligand (PD-L1) expression in stage II and III lung adenocarcinomas and nodal metastases. *J Thorac Oncol*. 2017;12:458-466.

11. Munari E, Zamboni G, Marconi M, et al. PD-L1 expression heterogeneity in non-small cell lung cancer: evaluation of small biopsies reliability. *Oncotarget*. 2017;8:90123-90131.

12. Sheng J, Fang W, Yu J, et al. Expression of programmed death ligand-1 on tumor cells varies pre and post chemotherapy in non-small cell lung cancer. *Sci Rep*. 2016;6:1-9.

13. Bailly C, Cléry P-F, Faivre-Chauvet A, et al. Immuno-PET for clinical theranostic approaches. *Int J Mol Sci*. 2016;18:57.

14. van der Veen EL, Bensch F, Glaudemans AWJM, Lub-de Hooge MN, de Vries EGE. Molecular imaging to enlighten cancer immunotherapies and underlying involved processes. *Cancer Treat Rev*. 2018;70:232-244.

15. Lipovsek D. Adnectins: engineered target-binding protein therapeutics. *Protein Eng Des Sel*. 2011;24:3-9.

16. Donnelly DJ, Smith RA, Morin P, et al. Synthesis and biologic evaluation of a novel 18F-labeled adnectin as a PET radioligand for imaging PD-L1 expression. *J Nucl Med*. 2018;59:529-535.

17. Lee S-J, Jang B-C, Lee S-W, et al. Interferon regulatory factor-1 is prerequisite to the

constitutive expression and IFN-gamma-induced upregulation of B7-H1 (CD274). *FEBS Lett*. 2006;580:755-62.

18. Caumanns JJ, van Wijngaarden A, Kol A, et al. Low-dose triple drug combination targeting the PI3K/AKT/mTOR pathway and the MAPK pathway is an effective approach in ovarian clear cell carcinoma. *Cancer Lett*. 2019;461:102-111.

19. Stutvoet TS, Kol A, de Vries EG, et al. MAPK pathway activity plays a key role in PD-L1 expression of lung adenocarcinoma cells. *J Pathol*. 2019;249:52-64.

20. Gonzalez Trotter DE, Meng X, McQuade P, et al. In vivo imaging of the programmed death ligand 1 by ^{18}F positron emission tomography. *J Nucl Med*. 2017;58:jnumed.117.191718.

21. Natarajan A, Patel CB, Ramakrishnan S, Panesar PS, Long SR, Gambhir SS. A novel engineered small protein for positron emission tomography imaging of human programmed death ligand-1: validation in mouse models and human cancer tissues. *Clin Cancer Res*. 2019;25:1774-1785.

22. Kumar D, Lisok A, Dahmane E, et al. Peptide-based PET quantifies target engagement of PD-L1 therapeutics. *J Clin Invest*. 2019;129:616-630.

23. Lv G, Sun X, Qiu L, et al. PET imaging of tumor PD-L1 expression with a highly specific nonblocking single-domain antibody. *J Nucl Med*. 2020;61:117-122.

24. Maute RL, Gordon SR, Mayer AT, et al. Engineering high-affinity PD-1 variants for optimized immunotherapy and immuno-PET imaging. *Proc Natl Acad Sci*. 2015;112:E6506-E6514.

25. Broos K, Keyaerts M, Lecocq Q, et al. Non-invasive assessment of murine PD-L1 levels in syngeneic tumor models by nuclear imaging with nanobody tracers. *Oncotarget*.

2017;8:41932-41946.

26. Garcia-Diaz A, Shin DS, Moreno BH, et al. Interferon receptor signaling pathways regulating PD-L1 and PD-L2 expression. *Cell Rep*. 2017;19:1189-1201.

27. Maleki Vareki S, Chen D, Di Cresce C, et al. IDO downregulation induces sensitivity to pemetrexed, gemcitabine, FK866, and methoxyamine in human cancer cells. Ahmad A, ed. *PLoS One*. 2015;10:e0143435.

28. Hettich M, Braun F, Bartholomä MD, Schirmbeck R, Niedermann G. High-resolution PET imaging with therapeutic antibody-based PD-1/PD-L1 checkpoint tracers. *Theranostics*. 2016;6:1629-1640.

29. Li C-W, Lim S-O, Xia W, et al. Glycosylation and stabilization of programmed death ligand-1 suppresses T-cell activity. *Nat Commun*. 2016;7:12632.

30. Horita H, Law A, Hong S, Middleton K. Identifying regulatory posttranslational modifications of PD-L1: a focus on monoubiquitination. *Neoplasia*. 2017;19:346-353.

31. Mezzadra R, Sun C, Jae LT, et al. Identification of CMTM6 and CMTM4 as PD-L1 protein regulators. *Nature*. 2017;549:106-110.

32. Varthaman A, Moreau HD, Maurin M, Benaroch P. TLR3-induced maturation of murine dendritic cells regulates CTL responses by modulating PD-L1 trafficking. *PLoS One*. 2016;11:1-15.

33. Wu Y, Chen W, Xu ZP, Gu W. PD-L1 distribution and perspective for cancer immunotherapy—blockade, knockdown, or inhibition. *Front Immunol*. 2019;10:2022.

34. Bensch F, van der Veen EL, Lub-de Hooge MN, et al. ^{89}Zr-atezolizumab imaging as a non-invasive approach to assess clinical response to PD-L1 blockade in cancer. *Nat Med*.

1 2018;24:1852-1858.

2 35. Niemeijer AN, Leung D, Huisman MC, et al. Whole body PD-1 and PD-L1 positron emission

3 tomography in patients with non-small-cell lung cancer. *Nat Commun*. 2018;9:4664.

4 36. Magzoub M, Jin S, Verkman AS. Enhanced macromolecule diffusion deep in tumors after

5 enzymatic digestion of extracellular matrix collagen and its associated proteoglycan

6 decorin. *FASEB J*. 2007;22:276-284.

7

1 **FIGURES**

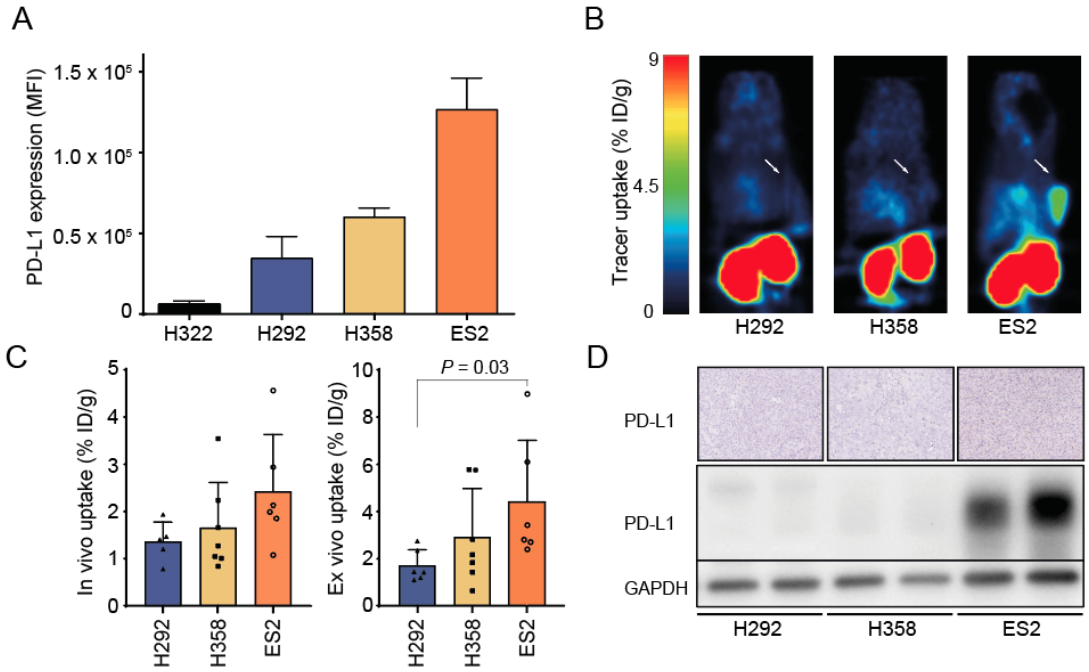

2

3 **FIGURE 1.** PD-L1 expression correlates with tracer uptake. **(A)** Basal PD-L1 membrane

4 expression of a panel of *in vitro* cultured cell lines as determined with flow cytometry. **(B)** *In vivo*

5 tracer distribution in %ID/g 60 minutes after injection of ^{18}F-BMS-986192 in BALB/c nude mice

6 with subcutaneous H292, H358 or ES2 tumors. The white arrow indicates the location of the

7 tumor. **(C)** *In vivo* and *ex vivo* ^{18}F-BMS-986192 uptake in xenografts 60 minutes after tracer

8 injection. **(D)** Tumor PD-L1 expression levels were analyzed using immunohistochemistry and **(E)**

9 Western blotting. Data is presented as mean + SD.

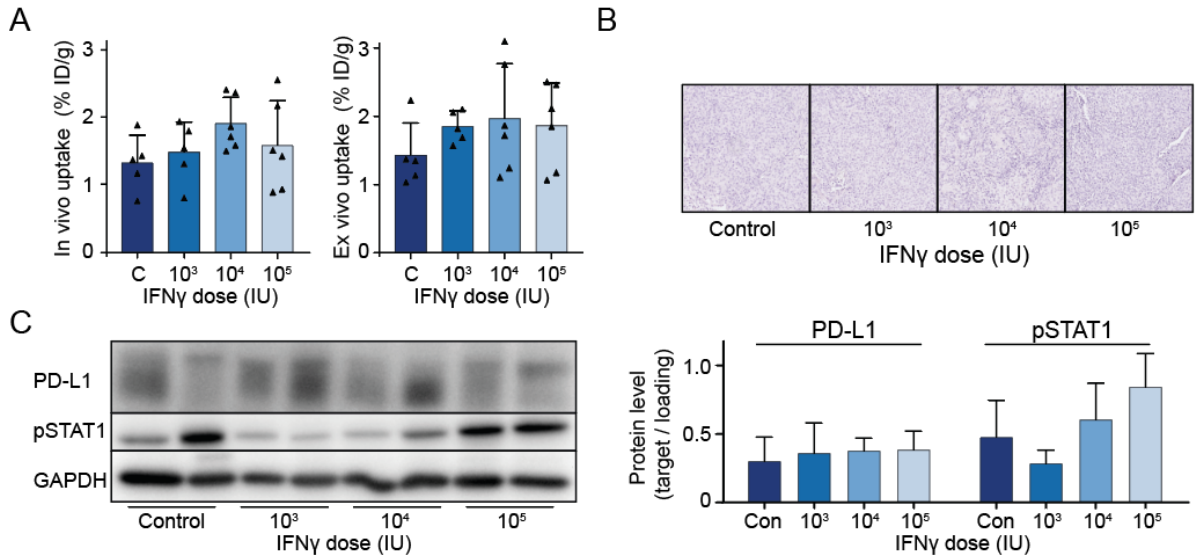

FIGURE 2. IFNγ fails to induce PD-L1 expression *in vivo*. **(A)** *In vivo* and *ex vivo* tracer uptake in %ID/g 60 minutes after injection of ^{18}F-BMS-986192 in BALB/c nude mice, with subcutaneous H292 xenografts treated with IFNγ once daily for 3 days by intraperitoneal injection. **(B)** H292 xenograft PD-L1 expression after treatment with different doses of IFNγ was measured using immunohistochemistry and **(C)** Western blotting. PD-L1 and pSTAT1 were measured in triplicate and quantified relative to the GAPDH. Data is presented as mean + SD.

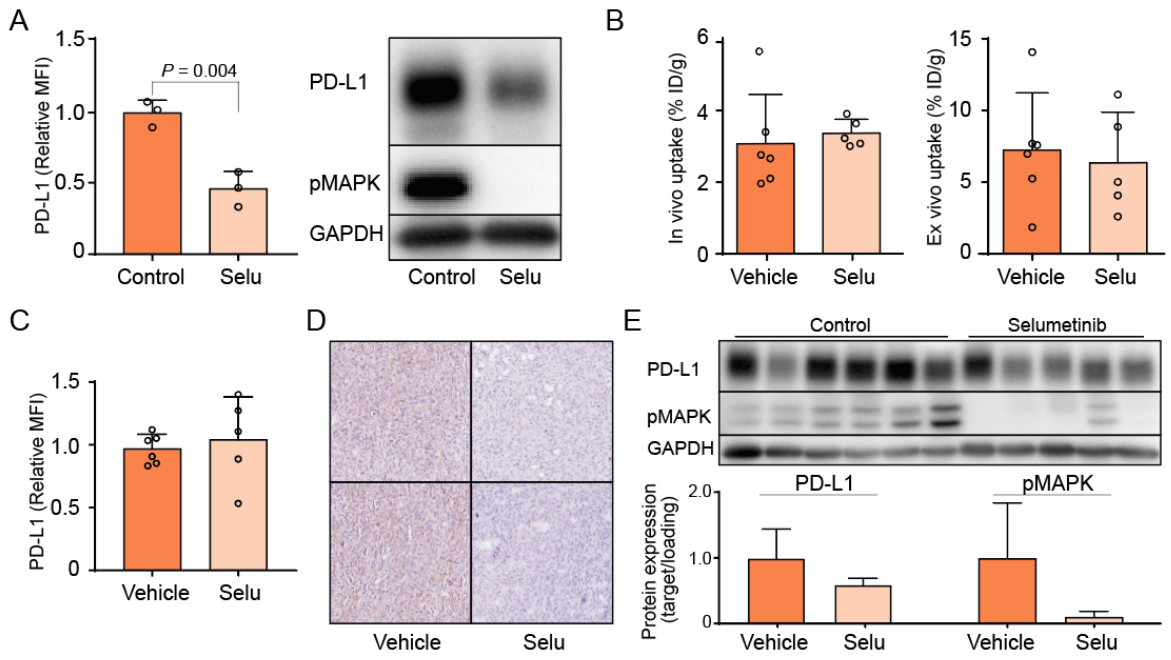

FIGURE 3. Selumetinib decreased PD-L1 expression *in vitro* and *in vivo*. **(A)** ES2 cells were treated *in vitro* with 10 µM selumetinib for 24 hours, followed by flow cytometry and Western blotting of PD-L1 membrane and total protein expression and MAPK signaling. **(B)** *In vivo* and e*x vivo* tracer uptake in %ID/g 60 minutes after injection of ^{18}F-BMS-986192 in BALB/c nude mice, with subcutaneous ES2 tumors and treated two times with 10 mg/kg selumetinib for 24 hours by oral gavage. **(C)** Tumor cell PD-L1 levels were measured using flow cytometry, **(D)** immunohistochemistry and **(E)** Western blotting. Additionally, pMAPK and PD-L1 were quantified by measuring their signal relative to the GAPDH signal. Data is presented as mean + SD. Abbreviations used: pMAPK = phosphorylated mitogen-activated protein kinase

SUPPLEMENTAL DATA

Supplementary Methods

Tracer Production. ^{18}F-BMT-187144 was produced as a precursor for the synthesis of ^{18}F-BMS-986192 using a Zymark robotic system. ^{18}F-fluoride was produced by irradiation of ^{18}O-H_2O with an IBA Cyclone 18 twin cyclotron via the ^{18}O(p,n)^{18}F nuclear reaction. The aqueous ^{18}F-fluoride was passed through a Sep-Pak light QMA anion exchange cartridge (Waters, Netherlands) to recover the ^{18}O-enriched water. ^{18}F-fluoride was then eluted from the cartridge with 1 mg of potassium carbonate (K_2CO_3, Sigma-Aldrich) in 1 mL of water for injections (in-house) and collected in a vial with 15 mg of Kryptofix [2.2.2] (Merck). To the vial, 1 mL of dry acetonitrile (MeCN, Rathburn) was added and the solvents were evaporated at 130 °C. The radioactive residue (^{18}F-KF-Kryptofix complex) was dried three times by addition and evaporation of anhydrous MeCN (3x 0.5 mL at 130 °C). To the dried ^{18}F-KF-Kryptofix complex, 0.5 mL of BMT-180478 (4 mg/ml in DMSO, Bristol-Meyers Squibb) was added and was allowed to react at 120°C for 10 minutes. The mixture was then diluted in 1.5 mL of water for injections and purified by high-performance liquid chromatography (HPLC) using an Elite LaChrom Hitachi L-7100 pump system with a Luna column (5 µm, 250 mm × 10 mm) equipped with both ultraviolet (UV) detection (Elite LaChrom VWR L-2400 UV detector set at 254 nm; Hitachi) and a Bicron radioactivity monitor. The product was eluted using a mobile phase of 32% MeCN in water with 0.1% trifluoroacetic acid (TFA, Sigma-Aldrich) and a flow rate of 4.6 mL/minute. The radioactive product, with a retention time of ~22 minutes, was collected in 80 mL water. The solution was then applied to a SepPak tC18 cartridge (Waters) and washed twice with 5 mL of water. The final product was eluted with 2 mL of ethanol and collected in a 2.5 mL conical vial.

Then ^{18}F-BMT-187144 was transferred to another hot cell equipped with a PharmTracer Eckert & Ziegler synthesis module. After drying of ^{18}F-BMT-187144, 0.3 mL of a solution of BMT-192920 precursor (4 mg/mL in DMSO, Bristol-Meyers Squibb) was added, followed by the addition of 0.1 mL water for injections. The mixture was allowed to react at 40 °C for 40 minutes. After cooling to 25 °C, the reaction mixture was transferred to the HPLC injection vial. The reaction vial was then washed with 1 mL of water for injections, which was then also transferred to the HPLC injection vial. The diluted reaction mixture was purified by HPLC using a Yarra SEC-3000 column (5 µm, 300 mm × 7.8 mm) and 100% phosphate buffered saline as mobile phase with a flow rate of 1.2 mL/minute. ^{18}F-BMS-986192, with a retention time of approximately 10 minutes, was collected into a 25 mL sterile vial (Mallinckrodt) via a sterilization filter (Millex-LG filter, 25 mm diameter, 0.2 µm pore size, polytetrafluoroethylene membrane, Millipore). An additional 6 mL phosphate buffered saline was added to the sterile vial to obtain a total volume of approximately 8 mL. Ultra-performance liquid chromatography was used for analysis of (radio)chemical purity, radiochemical identity and molar activity. For this, a Waters Acquity H-Class system and a BEH Phenyl column (1.7 µm; 3.0 mm x 50 mm) was used, equipped with both an UV detector (operated at 280 nm) and a radioactivity detector (Berthold FlowStar LB513, Mx50-6 flow cell). Gradient elution with a mixture of 0.1% aqueous TFA in ultrapure water (solvent A) and 0.1% TFA in mass spectrometry-grade acetonitrile (solvent B) was performed at a flow of 0.8 mL/min. The following gradient profile was used: 0-6 min 10-50% B, 6-8 min 50-70% B, 8-10 min 70-10% B. Retention times were 3.1 min for ^{18}F-BMT-187144 and 5.3 min for ^{18}F-BMS-986192.

1 **Supplementary Figures**

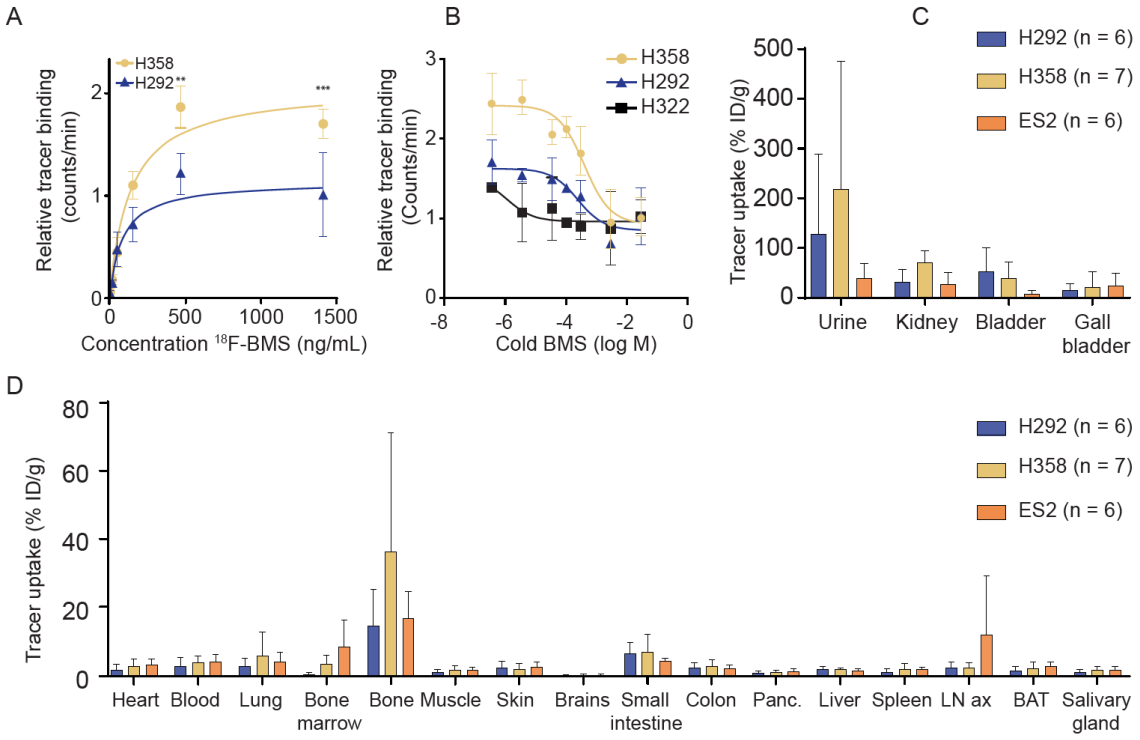

2

3 **SUPPLEMENTAL FIGURE 1.** *In vitro* tracer binding and biodistribution of ^{18}F-BMS-986192 in

4 xenograft models. **(A)** ^{18}F-BMS-986192 was added to H292 or H385 cells and incubated for 60

5 minutes at 37°C. After washing, the remaining bound counts were measured using a gamma

6 counter. Binding assays were performed in triplicate. Data is expressed relative compared to

7 H292 with the highest tracer concentration. Differences were tested using ANOVA with

8 bonferroni's multiple comparisons test, ** $p < 0.01$, *** $p < 0.001$. **(B)** H358, H292 and H322

9 cells were incubated with 1 MBq (corresponding to 167 ng) ^{18}F-BMS-986192 for 60 minutes at

10 37°C together with increasing concentrations of unlabeled precursor. After washing, bound

11 counts were measured using a gamma counter. Binding assays were performed in triplicate and

12 data was expressed relative to the signal of the highest blocking dose. **(C)** A 60 minute dynamic

13 PET scan was performed using ^{18}F-BMS-986192 in BALB/c nude mice with established H292,

H358, or ES2 xenograft tumors, followed by *ex vivo* biodistribution studies. Tracer uptake in excretion organs and **(D)** other organs was assessed by measuring counts per minute in a gamma counter. Uptake is expressed as percentage of injected dose per gram (%ID/g). Panc. = pancreas, LN ax = axial lymph node, BAT = brown adipose tissue. Data is presented as mean +/± SD.

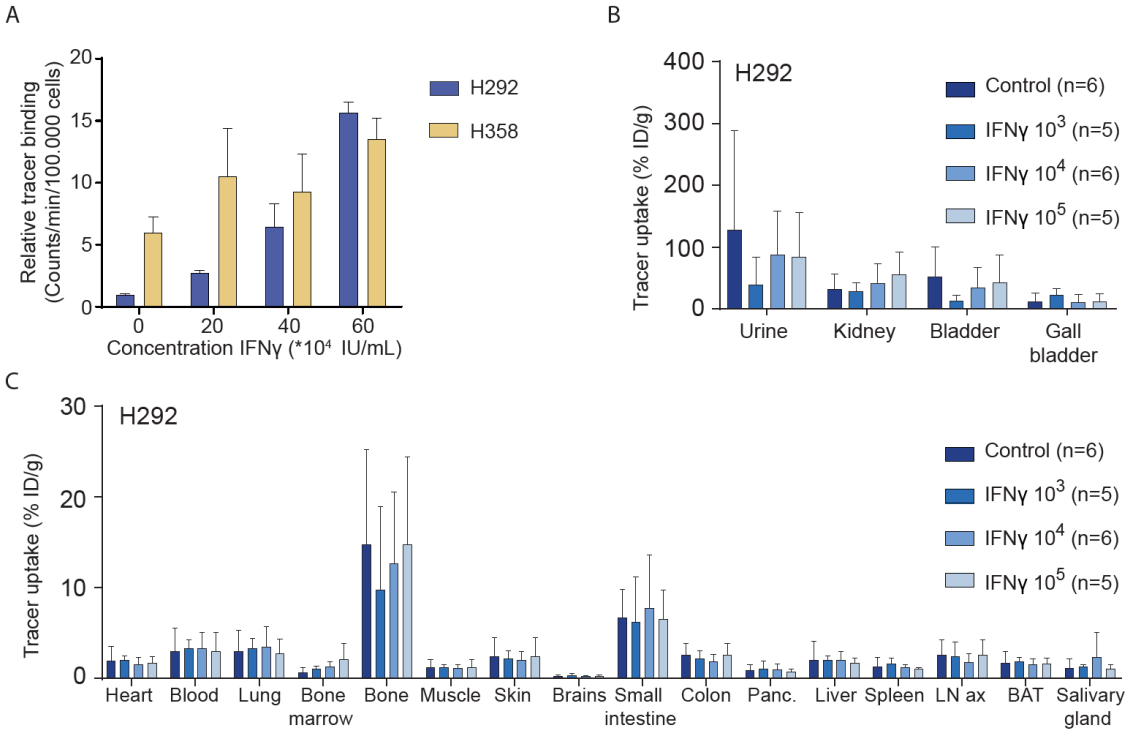

SUPPLEMENTAL FIGURE 2. IFNγ does not influence biodistribution of ^{18}F-BMS-986192 *in vivo*. **(A)** H292 and H358 cells were treated with a range of IFNγ concentrations for 24 hours. Tracer binding/100,000 cells was measured using a gamma counter and expressed relatively to untreated H292. BALB/c nude mice with established H292 xenograft tumors were randomized between control and different IFNγ doses (n= 5/6 per group). After 3 days treatment by intraperitoneal injection, a 60-min dynamic PET scan was performed using ^{18}F-BMS-986192, followed by *ex vivo* biodistribution studies. Tracer uptake in **(B)** excretion organs and **(C)** other organs was assessed *ex vivo* by measuring counts per minute in a gamma counter. Uptake is expressed as percentage of injected dose per gram (%ID/g). Panc. = pancreas, LN ax = axial lymph node, BAT = brown adipose tissue. Data is presented as mean + SD.

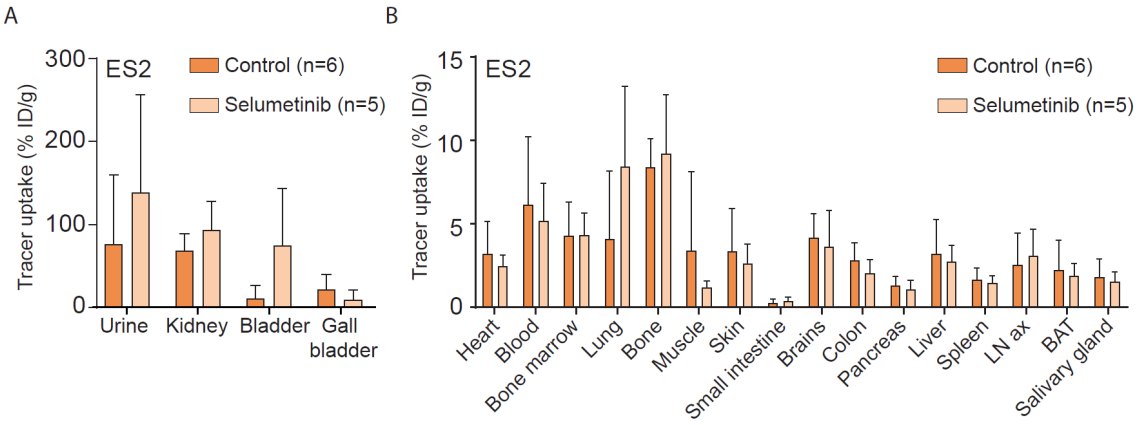

SUPPLEMENTAL FIGURE 3. Selumetinib does not influence biodistribution of ^{18}F-BMS-986192 *in vivo*. BALB/c nude mice with established ES2 xenograft tumors were randomized between control and selumetinib treatment (n= 5/6 per group). After 24 hours treatment by oral gavage, a 60-min dynamic PET scan was performed using ^{18}F-BMS-986192, followed by *ex vivo* biodistribution studies. Tracer uptake in **(A)** excretion organs and **(B)** other organs was assessed *ex vivo* by measuring counts per minute in a gamma counter. Uptake is expressed as percentage of injected dose per gram (%ID/g). LN ax = axial lymph node, BAT = brown adipose tissue. Data is presented as mean + SD.

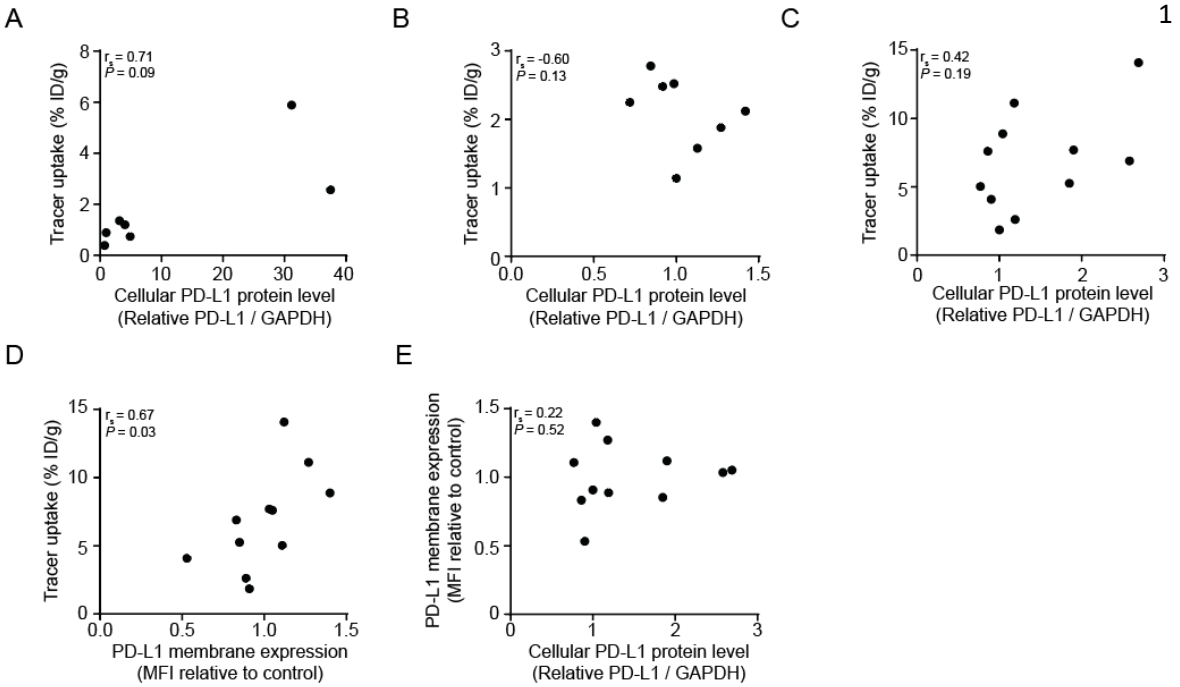

SUPPLEMENTAL FIGURE 4. Relation of PD-L1 protein and membrane expression with tracer uptake. **(A)** Correlation of PD-L1 protein levels in Figure 1D, with *ex vivo* tracer uptake. **(B)** Correlation of PD-L1 protein levels in Figure 2C, with *ex vivo* tracer uptake. **(C)** Correlation of PD-L1 protein levels in Figure 3E, with *ex vivo* tracer uptake. **(D)** Correlation of PD-L1 membrane expression in Figure 3C, with *ex vivo* tracer uptake. **(E)** Correlation of PD-L1 membrane expression in Figure 3C with PD-L1 protein levels in level 3E. r_s = Spearman's correlation.